International Journal of Greenhouse Gas Control 35 (2015) 131–137

Contents lists available at ScienceDirect

International Journal of Greenhouse Gas Control

journal homepage: www.elsevier.com/locate/ijggc

Understanding the solubility of water in carbon capture and storage mixtures: An FTIR spectroscopic study of $H_2O + CO_2 + N_2$ ternary mixtures

Stéphanie Foltran[a], Matthew E. Vosper[a], Norhidayah B. Suleiman[a], Alisdair Wriglesworth[a], Jie Ke[a], Trevor C. Drage[b], Martyn Poliakoff[a], Michael W. George[a,c,*]

[a] School of Chemistry, The University of Nottingham, University Park, Nottingham NG7 2RD, UK
[b] Department of Chemical and Environmental Engineering, The University of Nottingham, University Park, Nottingham NG7 2RD, UK
[c] Department of Chemical and Environmental Engineering, University of Nottingham Ningbo China, 199 Talking East Road, Ningbo 315100, China

ARTICLE INFO

Article history:
Received 28 August 2014
Received in revised form 4 February 2015
Accepted 5 February 2015

Keywords:
Carbon capture and storage
Infrared spectroscopy
Phase behaviour
Carbon dioxide
Water
Pipeline

ABSTRACT

The solubility of water (H_2O) in carbon dioxide (CO_2) and nitrogen (N_2) mixtures (x_{N2} = 0.050 and 0.100, mole fraction) has been investigated at 25 and 40 °C in the pressure range between 8 and 18 MPa. The motivation for this work is to aid the understanding of water solubility in complex CO_2-based mixtures, which is required for the safety of anthropogenic CO_2 transport *via* pipeline for carbon capture and storage (CCS) technology. The measurements have been performed using an FTIR spectroscopic approach and demonstrate that this method is a suitable technique to determine the concentration of water in both pure CO_2 and $CO_2 + N_2$ mixtures. The presence of N_2 lowers the mole concentration of water in CO_2 by up to 42% for a given pressure in the studied conditions and this represents important data for the development of pipelines for CCS. This work also provides preliminary indications that the key parameters for the solubility of H_2O in such $CO_2 + N_2$ mixtures are the temperature and the overall density of the fluid mixture and not solely the given pressure of the CCS mixture. This could have implications for understanding the parameters required to be monitored during the safer transportation of CO_2 mixtures in CCS pipelines.

1. Introduction

CO_2 concentrations in the atmosphere have reached record levels (EASAC, 2013) and the implications for global warming are clearly of concern (Keeling et al., 1995). Carbon capture and storage (CCS) (Keith, 2009; Haszeldine, 2009) is currently one of the leading technologies for addressing the problem in the short and medium term. The ultimate ambition of CCS is to help reduce CO_2 emissions by 90% by 2050 and CCS pilots are already operating in the USA and Europe, achieving localised reductions in emissions of ca. 16% in 2011 (IEA, 2012). Much of the CCS literature has understandably focused on CO_2 capture (Goeppert et al., 2012; Lee et al., 2012; Markewitz et al., 2012; Nielsen et al., 2012; Rubin et al., 2012) but there are factors still required to address safety issues in the overall CCS process particularly transportation of CO_2 from power plant to the sub-surface reservoirs.

The majority of proposed CCS schemes involve transport via pipelines, which represents a more cost-effective and safer approach than ship transport (Herzog, 2011). Pipeline networks are likely to be constructed of carbon steel rather than stainless steel on grounds of cost (Buit et al., 2011), with the result that possible corrosion of the pipes is an important issue (Choi and Nesic, 2011; Choi et al., 2010; Cui et al., 2006; Xiang et al., 2006). All of the common capture approaches (post-combustion, oxy-fuel or pre-combustion) can give rise to impurities in the final CO_2 stream including water in addition to other permanent gases (such as N_2, H_2 or Ar) up to 4 vol.%, depending on the different capture technologies (Abbas et al., 2013; Davison and Thambimuthu, 2009; de Visser et al., 2008; Pipitone and Bolland, 2009; Stevens et al., 2011). The presence of water is a powerful cause of the CO_2 pipeline corrosion, particularly if the water accumulates as liquid at points within the pipes. Therefore, to avoid the separation of liquid H_2O from the CO_2 stream during the transport stage, the water content in the CO_2 stream must be below the solubility of water under various operating conditions, including changes in temperature, pressure and impurity concentrations. The effect of impurities (e.g.

* Corresponding author at: School of Chemistry, The University of Nottingham, University Park, Nottingham NG7 2RD, UK. Tel.: +44 115 951 3512.
E-mail address: mike.george@nottingham.ac.uk (M.W. George).

http://dx.doi.org/10.1016/j.ijggc.2015.02.002
1750-5836/

Nomenclature

C_{H_2O}	concentration of water (mol dm^{-3})
P	pressure (MPa)
SD(C_{H_2O})	standard deviation from the concentration of water
SD(y_{H_2O})	standard deviation from the mole fraction of water
T_c	critical temperature (°C)
$V^{sat}_{H_2O}$	saturation volume of water (μL)
y_{H_2O}	mole fraction of water
y_{N_2}	mole fraction of nitrogen

Greek letters

ν_2	bending frequency of water
ρ	density (mol dm^{-3})

N_2, H_2, etc.) on the solubility of water in anthropogenic CO_2 will provide guidance on the maximum allowable water content in the CO_2 streams for pipeline CO_2 transport.

There have been many studies on the solubility of water in pure CO_2 (Bamberger et al., 2000; Briones et al., 1987; Coan and King Jr., 1971; D'Souza et al., 1988; Gillespie and Wilson, 1982; Hou et al., 2013; Jackson et al., 1995; King et al., 1992; Koglbauer and Wendland, 2008; Sako et al., 1991; Song and Kobayashi, 1986; Spycher et al., 2003; Valtz et al., 2004; Wang et al., 2012; Wiebe, 1941) but there are very few reports on solubility in more complex mixtures such as the ternary systems of $H_2O + CO_2$ + impurities (Adisasmito et al., 1991; Austegard et al., 2006; Liu et al., 2012; Song and Kobayashi, 1990) and none of these studies address the solubility of water in anthropogenic CO_2. This is important because impurities can significantly change the thermodynamic properties of CO_2. For example, we recently reported studies on the density of $CO_2 + N_2$ and $CO_2 + H_2$ mixtures, highlighting how even a low percentage of N_2 or H_2 can induce significant reductions in the density near to the mixture critical point (Sanchez-Vicente et al., 2013).

Here we report the solubility of water in the dense phase of the $CO_2 + N_2$ mixtures to try to establish the effect of N_2 on the solubility of H_2O in CO_2 under conditions relevant to CCS. N_2 is one of the most common impurities in the CCS process (IEAGHG, 2011). The level of N_2 present in the CO_2 streams can be very low (e.g. 0.1 vol.% from the post-combustion process). However, under upset conditions, the concentration of N_2 may rise significantly to a level of 5–10 vol.%.

All of our measurements have been carried out in situ using custom-built high pressure equipment coupled to an FTIR spectrometer. There have been previous reports describing the use of FTIR spectroscopy to study the solubility of H_2O in pure CO_2 (Jackson et al., 1995; Koglbauer and Wendland, 2008; Wang et al., 2012) and FTIR spectroscopy has already been extensively used for the study of solutes in supercritical fluids (Buback, 1995; Kazarian et al., 2000; Poliakoff et al., 1995). Furthermore, infrared spectroscopy is highly sensitive to water, making the technique highly suitable to determine trace amounts of water in compressed gases. More specifically in this paper, we focus on the intense absorption band of water in the mid-IR region (ca. 1600 cm^{-1}), which gives high sensitivity even for low concentrations of H_2O. Initially, we validate our method by measuring the solubility of water in pure CO_2 where the results can be benchmarked against existing literature data (Gillespie and Wilson, 1982; King et al., 1992; Song and Kobayashi, 1986; Spycher et al., 2003; Wiebe, 1941) under the same conditions. Then we use FTIR spectroscopy to measure the solubility of water in CO_2 + 5% N_2 and CO_2 + 10% N_2 mixtures at 298.15 K (25 °C) and 313.15 K (40 °C) over the pressure range 8–18 MPa.

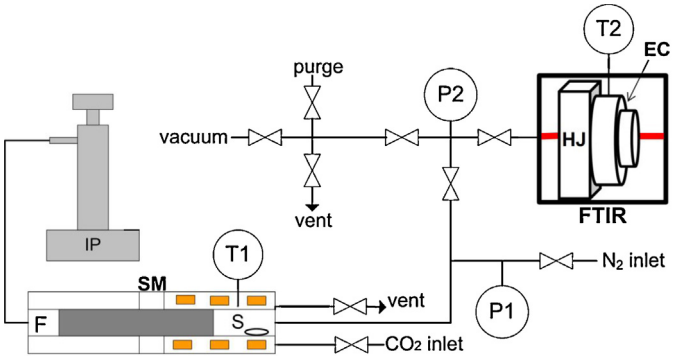

Fig. 1. High pressure–high temperature controlled set-up combined with an FTIR spectrometer: the components are labelled as followed: IP, Isco syringe pump; F, transmitting fluid; S, sampling chamber; T1, temperature controller for the gas mixer; P1, pressure transducer (0–2 MPa); T2, temperature controller for the infrared cell; P2, pressure transducer (0–34 MPa); HJ, heating jacket; EC, infrared equilibrium cell.

2. Materials and methods

2.1. Chemicals

Ultra-high purity water was obtained from a Milli-Q® Advantage A10 unit with a resistivity of 18.2 MΩ cm at 25 °C and a total organic carbon (TOC) content ≤5 μg dm^{-3}. CO_2 was SFC grade with a purity of 99.99% and supplied by BOC. Oxygen-free nitrogen gas with a purity of 99.9995% was also purchased from BOC.

2.2. Apparatus

The FTIR spectroscopic measurements were performed using a Nicolet 380 spectrometer equipped with a deuterated triglycine sulphate detector. Single beam spectra were recorded with a 4 cm^{-1} resolution and were obtained after the Fourier transformation of 32 accumulated interferograms. Fig. 1 gives a schematic representation of the apparatus used in this work.

The infrared optical cell, built in-house, has been described in detail previously (Poliakoff et al., 1995). Briefly, it is a stainless steel cell composed of two CaF_2 windows with an optical path length of 3 mm. The windows and window holders are sealed to the body of the cell using epoxy resin and the cell is sealed with a Teflon O-ring. A heating jacket fits around the cell controlling the temperature inside to within ± 0.3 °C. The cell temperature is monitored by a K-type thermocouple, which is in direct contact with the sample inside the cell.

The $CO_2 + N_2$ mixtures were prepared using a stainless steel sample mixer. The mixer consists of a variable-volume sample chamber separated by a piston from a second chamber filled with a pressurising fluid, in this case isopropyl alcohol (IPA). The system is connected to an Isco syringe pump which allows pumping or withdrawal of IPA to move the piston and, hence, to regulate the volume of the sample chamber. The mixer has a custom built mixing mechanism and a heating jacket monitored by a K-type thermocouple mounted in the chamber wall. The pressure inside the sample mixer is measured by two SuperTJE pressure transducers (RDP Electronics Ltd.) with maximum pressure ratings of 2 and 34.5 MPa, respectively, and a stated accuracy of ±0.05% of full scale. The sample mixer has been described in detail elsewhere (Ke et al., 2014).

2.3. Experimental procedure

A $CO_2 + N_2$ mixture was prepared in the sample mixer at room temperature according a method already used in our group

(Sanchez-Vicente et al., 2013). N_2 was first injected into the mixer to a preset pressure, measured by the pressure transducer P1 (see Fig. 1). The NIST webbook of chemistry database (NIST, 2014) was used to determine the density of N_2 and hence, to calculate the amount of CO_2 needed to make up a mixture of a given composition. After a given amount of CO_2 was loaded into the sample mixer, the mixture was then heated to the desired temperature and its pressure was increased to ~10 MPa. The mixture was left stirring for 2 h to ensure homogeneity prior to use in the IR measurements.

The water was first injected to the bottom of the IR cell using either a 1 μL or a 5 μL micro-syringe with an accuracy of 2%. After the cell was sealed, it was preheated to the desired temperature. The gas mixture was finally introduced into the IR cell from the sample mixer. The resulting $H_2O + CO_2 + N_2$ mixture in the IR cell was stirred for ca. 2 min before collecting the first FTIR spectrum. Following this, FTIR spectra were then recorded every 5 min until equilibrium was achieved. As the amount of water introduced into the cell is very small (<2 μL), only the CO_2 phase appears in the space between the two IR windows even when both the water and CO_2 phases coexist in the cell. The concentration of H_2O in the CO_2 phase of the $H_2O + CO_2 + N_2$ mixture was established using the method described below.

3. Results and discussion

3.1. FTIR spectra

Fig. 2 shows a typical FTIR spectrum in the region of interest for this work. The band is assigned to the ν_2 bending mode of water at 1600 cm^{-1}, although the IR absorbance is lower than the value corresponding to the saturated concentration of H_2O under these conditions. Our investigations have focused on using this band to determine the saturation of H_2O in mixtures of relevance to CCS.

Fig. 3(a) displays the increase in absorbance of the water bending mode as a function of the volume of water added. These spectra were obtained after subtraction of the CO_2 bands. It is clear that the absorbance of the H_2O band increases with the volume of water added until a threshold is reached, where the absorbance of the H_2O band remains constant as no further water can be dissolved in the CO_2-rich phase. Under these conditions, the CO_2-rich phase is considered to be saturated with water.

In order to determine the saturation volume of water accurately, the absorbance of the water ν_2 band is plotted as a function of the volume of the water at a given temperature and pressure (Fig. 3(b)). The calibration curve is fitted with a linear line, and the

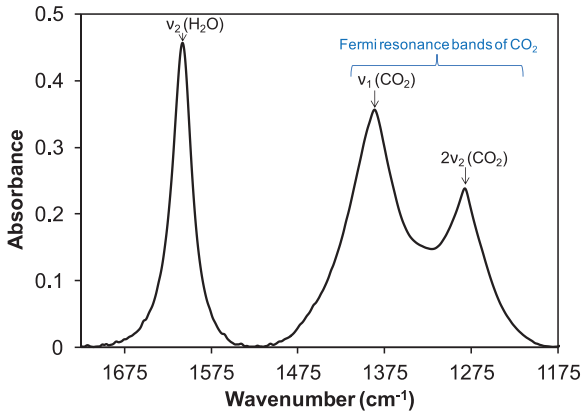

Fig. 2. FTIR spectrum of H_2O in CO_2 + 5% N_2 at 40 °C, 12.41 MPa and with 0.5 μL of H_2O: the bending mode of water has been used to determine the amount of water in the $CO_2 + N_2$ mixtures, since the band is not obscured by the Fermi resonance bands of CO_2 at 1550–1250 cm^{-1}.

horizontal line in the saturation region represents the average of the absorbance of the water peak with various amounts of injected water. The saturation volume of H_2O ($V^{sat}_{H_2O}$) can be determined from the absorbance measured in the saturation region (red solid circles in Fig. 3(b)) and the calibration curve (blue solid circles in Fig. 3(b)).

The water solubility, expressed as the molar concentration of H_2O in the CO_2 phase (C_{H_2O}) can be calculated from $V^{sat}_{H_2O}$, the density of pure H_2O at room temperature (taken as 1.00 g cm^{-3}) and the volume of the IR cell, calibrated prior to any measurements. The measurements with various amounts of injected water have been made in the saturation region at a fixed pressure. The evolution of the absorbance as a function of the volume of water for each pressure studied is shown in Fig. 4. The average and the standard deviation of the water solubility obtained from these measurements are listed in Table 1 for each pressure.

3.2. Solubility of H_2O in pure CO_2 and in $CO_2 + N_2$ mixtures at 298.15 K (25 °C) and 313.15 K (40 °C)

The phase behaviour of ternary mixtures is complex and it was important to ensure that any measured effects on water solubility in the $CO_2 + N_2$ mixtures could be attributed to the presence of N_2 rather than any changes that may arise because of phase changes. We have chosen two levels of N_2 concentration in this study, i.e. 5 and 10% of N_2 in CO_2 (mole fraction). As mentioned in Section 1,

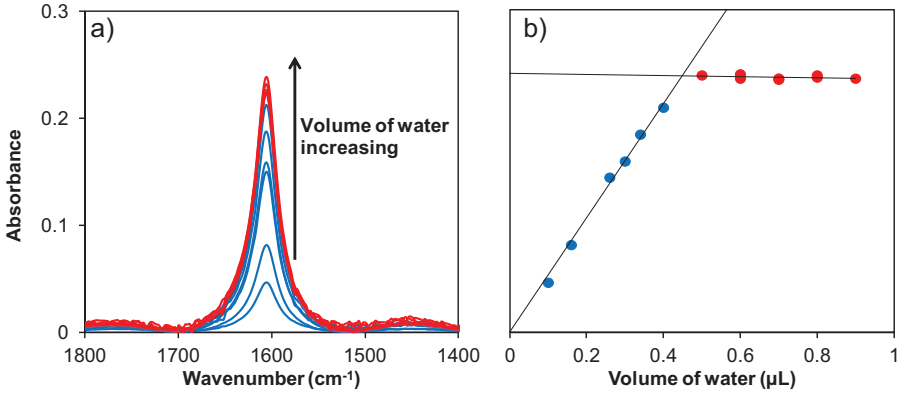

Fig. 3. (a) Evolution of the H_2O bending mode at 1600 cm^{-1} as a function of the volume of H_2O at 40 °C and 10.20 MPa, with corrections for the CO_2 spectra: blue spectra represent the calibration experiment; red spectra represent the saturation experiment. (b) Evolution of the absorbance of the H_2O band at 1600 cm^{-1} as a function of the volume of the water introduced in $CO_2 + N_2$ mixture at 40 °C and 10.20 MPa: blue dots represent the calibration data and the red dots represent the saturation data.

Table 1
Data obtained at 40 °C in pure CO_2, in CO_2 + 5% N_2 and CO_2 + 10% N_2 with C_{H_2O}, concentration of water in the mixture; SD(C_{H_2O}), standard deviation from the concentration of water in the mixture; y_{H_2O}, mole fraction of water in the mixture and SD(y_{H_2O}), standard deviation from the mole fraction of water in the mixture.

y_{N_2}	P (MPa)	ρ from REFPROP (mol dm^{-3})	N^a	C_{H_2O} (mol dm^{-3})	SD(C_{H_2O})	y_{H_2O} ($\times 10^3$)	SD(y_{H_2O}) ($\times 10^3$)
0.0994	8.90	5.97	18	0.0215	0.0006	3.60	0.08
0.0995	10.21	8.00	8	0.0270	0.0006	3.40	0.08
0.0990	11.14	9.65	4	0.0314	0.0005	3.34	0.02
0.0985	12.41	11.67	3	0.0441	0.0003	3.76	0.02
0.1000	13.79	13.21	3	0.0532	0.0004	4.04	0.04
0.1000	15.86	14.84	3	0.0620	0.0002	4.18	0.02
0.0990	17.24	15.67	3	0.0677	0.0002	4.32	0.02
0.0503	8.90	6.92	3	0.0271	0.0005	3.88	0.04
0.0500	10.21	10.25	3	0.0376	0.0001	3.73	0.02
0.0503	11.03	12.12	4	0.0471	0.0009	3.93	0.10
0.0500	12.41	14.13	3	0.0595	0.0001	4.24	0.01
0.0504	13.79	15.32	4	0.0685	0.0007	4.44	0.04
0.0504	15.86	16.51	3	0.0752	0.0003	4.55	0.01
0.0504	17.24	17.09	3	0.0797	0.0003	4.66	0.02
0.0000	8.27	7.13	3	0.0284	0.0003	4.01	0.04
0.0000	8.90	10.37	3	0.0407	0.0020	3.92	0.14
0.0000	10.21	14.61	3	0.0650	0.0009	4.45	0.07
0.0000	11.14	15.65	3	0.0720	0.0004	4.54	0.03
0.0000	12.41	16.56	3	0.0808	0.0010	4.81	0.06

[a] N, number of experiments.

these two mixtures represent the CO_2 streams in pipelines under conditions where upsets may occur in the capture stage. In addition, the solubility data in the CO_2 mixtures with a broad range of N_2 concentration are necessary to develop reliable thermodynamic models for predicting water solubility in impure CO_2. Such models will allow prediction of the water solubility in CO_2 with low level of N_2 (e.g. 0.1 vol.%). According to REFPROP (Lemmon et al., 2007), the critical temperature is T_c = 27.1 °C for the 5% N_2 mixture and T_c = 22.5 °C for the 10% N_2 mixture, respectively. Thus, to ensure that for all of the three systems (5% N_2, 10% N_2 and pure CO_2) there is only a single CO_2-rich phase coexisting with the water-rich phase in our measurements, the majority of our measurements have been carried out at 40 °C, which is well above the critical temperature of pure CO_2 and both binary mixtures. The experimental pressure range is between 8 and 18 MPa, which covers the pressure range recommended for dense phase CO_2 transportation pipelines in CCS processes. As the aim of this work is to show how the presence of the impurity (N_2 here) affects the solubility of water in CO_2 and to validate our FTIR spectroscopic method, the homogeneity of mixtures at 40 °C simplifies experiments and allows us to demonstrate the validity of our approach. Once the method had been validated, further measurements were made at 25 °C to explore the density effect on the water solubility in the CO_2 + N_2 mixtures.

3.2.1. *Evolution of the concentration of water as a function of the mixture pressure*

Initially we examined the solubility of water in pure CO_2 in order to validate our method. We found that C_{H_2O} at 40 °C in the pressure range 8.27–12.41 MPa varied from 0.0284 to 0.0808 mol dm^{-3} and increased with the pressure. The water solubility data published previously by King et al. (1992) were expressed as the mole fraction of H_2O in the CO_2 phase (y_{H_2O}). We therefore converted these data to molar concentration (Fig. 5) by using the CO_2 densities calculated from the Span–Wagner equation of state (Span and Wagner, 1996). As illustrated in Fig. 5, our measurements are in good agreement with the data reported by King et al. (1992), with errors ≤3%. The relative standard deviation of the reported measurements at each pressure under these conditions is <3.5%.

The solubility of H_2O in the CO_2 phase with 5% N_2 is also depicted in Fig. 5, showing that addition of 5% of N_2 to CO_2 causes a significant decrease in the molar concentration of the water in CO_2.

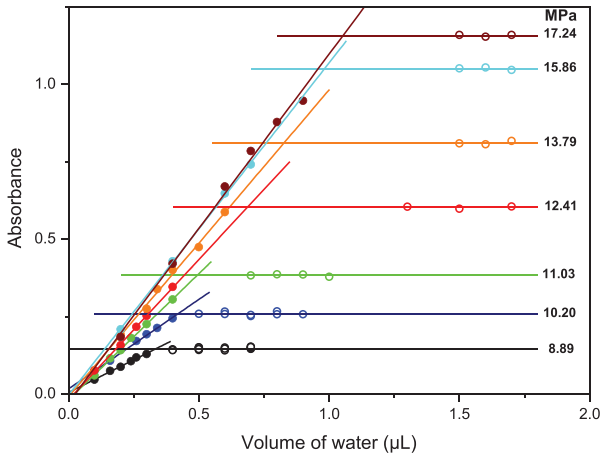

Fig. 4. Evolution of the absorbance of the H_2O band at 1600 cm^{-1} as a function of the volume of the water introduced in CO_2 + 10% N_2 mixture at 40 °C for a pressure range between 8.89 and 17.24 MPa.

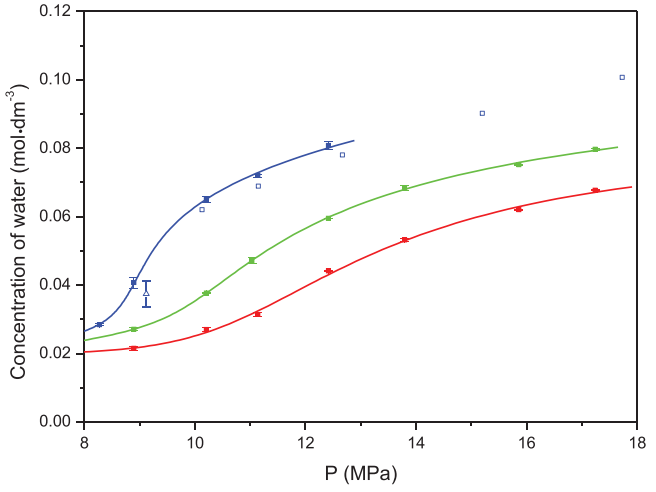

Fig. 5. Evolution of the molar concentration of water in: (■) pure CO_2 from this work; (□) pure CO_2 from King et al. (1992); (△) pure CO_2 from Wang et al. (2012); (■) CO_2 + 5% N_2; (■) CO_2 + 10% N_2 at 40 °C as a function of the pressure. The fitted lines have been drawn to guide the eyes.

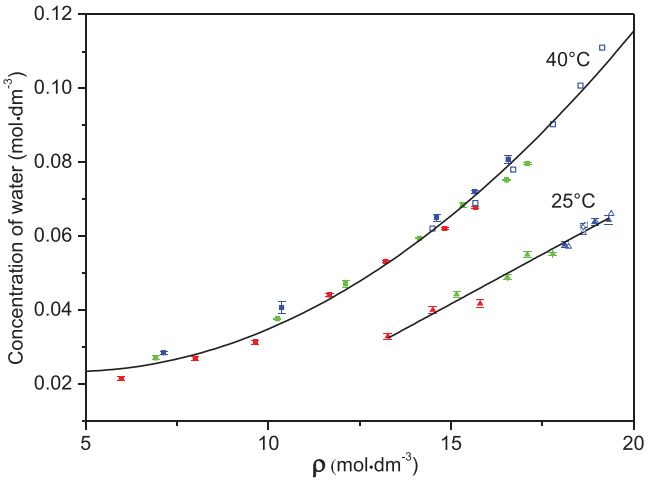

Fig. 6. Evolution of the molar concentration of water as a function of the density at: (■) 40 °C in pure CO_2 from this work; (□) 40 °C in pure CO_2 from King et al. (1992); (■) 40 °C in CO_2 + 5% N_2; (■) 40 °C in CO_2 + 10% N_2; (▲) 25 °C in pure CO_2 from this work; (△) 25 °C in pure CO_2 from King et al. (1992); (▽) 25 °C in pure CO_2 from Wiebe (1941); (○) 25 °C in pure CO_2 from Gillespie and Wilson (1982); (◁) 25 °C in pure CO_2 from Song and Kobayashi (1986); (▲) 25 °C in CO_2 + 5% N_2; (▲) 25 °C in CO_2 + 10% N_2. The curves are merely a guide to the eye.

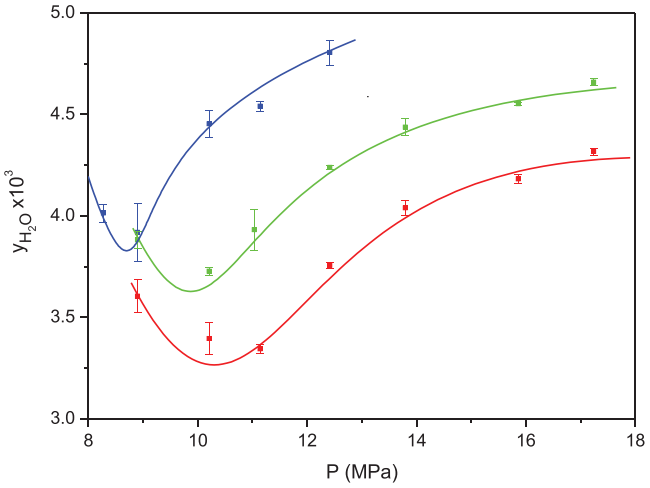

Fig. 7. Evolution of the mole fraction of water in: (■) pure CO_2; (■) CO_2 + 5% N_2; (■) in CO_2 + 10% N_2 at 40 °C as a function of the pressure. The three smoothed curves were obtained from fitted C_{H_2O} −ρ curves shown in Figures S1–S3 in Electronic Supplementary Materials. More details can be found from the text below.

For example, at 10.20 MPa the molar concentration is 42% lower in a mixture containing 5% N_2 than in pure CO_2. To investigate the effect of N_2 further, we have also studied mixtures CO_2 + 10% N_2, even though these levels of impurity are somewhat higher than would normally be expected in CCS. In this case, the concentration of water in the mixture is lowered by up to 59% at 10.20 MPa compared to the value in pure CO_2. The relative standard deviation of the reported experiments is <3% (see Table 1). Thus, these results highlight the detrimental impact of the N_2 on the solubility of water in CO_2. These results indicate that great care should be taken in evaluating the solubility of water in mixtures used for CCS and we have analysed this further by examining the effect of overall density rather than pressure on solubility of water in these mixtures.

3.2.2. Evolution of the concentration of water as a function of the density

Fig. 6 shows the molar concentration of water plotted as a function of the density for the different mixtures studied in this paper (pure CO_2; CO_2 + 5% N_2 and CO_2 + 10% N_2). The density of the CO_2 + N_2 mixtures has been calculated by using the GERG-2008 equation of state (Kunz and Wagner, 2012). This equation has proved to accurately describe the density of the CO_2 + N_2 mixtures; detailed comparisons between the predictions and the experimental density can be found from the literature (Kunz et al., 2007) and from our previous publication (Sanchez-Vicente et al., 2013). Interestingly, it can be clearly observed that at 40 °C and for a given density of the mixture, C_{H_2O} remains almost constant whatever the composition of the mixture. Indeed, all these data for the different mixtures can be fitted on the same trend line in a broad density range. This can be rationalised by the presence of N_2 noticeably reducing the density at a given pressure, which explains why the solubility of H_2O decreases when a higher molar percentage of N_2 is present, as observed in Fig. 5. In other words, for the same temperature–pressure value, the density can be very different for pure CO_2 as compared to CO_2 + 5% N_2 and CO_2 + 10% N_2 and this result the saturation values of water being significantly affected.

In order to explore the effect of density on the solubility of water further we have also performed preliminary measurements for H_2O + CO_2 + N_2 at 25 °C (Fig. 6). As mentioned previously, at 25 °C we are close to the critical point for the mixtures CO_2 + 5% N_2 (T_c = 27.1 °C) and CO_2 + 10% N_2 (T_c = 22.5 °C) and we must consider the phase behaviour. Indeed, the critical temperature of CO_2 (T_c = 31.1 °C) is lowered by the presence of N_2 and in this region the density of the mixture is very sensitive, hence, the temperature and the pressure need to be controlled accurately. As a consequence the uncertainties on our measurements are slightly larger than those obtained at 40 °C, which we attribute to the density changing rapidly in this region, so fewer data are reported in this study. Nevertheless, the results reported at 25 °C in Fig. 6 can give a clear indication of how C_{H_2O} changes with the density and the concentration of N_2 in CO_2. Similarly to the data at 40 °C where the three mixtures fit the same trend line, i.e. for a given density of the fluid, C_{H_2O} remains almost constant whatever the composition of the mixture.

The effect of N_2 on the density at 25 °C is even more significant than at 40 °C. Indeed, at 25 °C for the same range of pressure the densities of the different mixtures are very different. The density is comprised between 18.1 and 19.3 mol dm^{-3} for pure CO_2, between 15.2 and 17.8 mol dm^{-3} for CO_2 + 5% N_2 and between 13.3 and 15.8 mol dm^{-3} for CO_2 + 10% N_2.

3.2.3. Evolution of the mole fraction of water as a function of the pressure

The solubility of water can also be illustrated by using the mole fraction of water (y_{H_2O}). Fig. 7 shows the variation in the mole fraction of water in the mixtures as a function of the pressure. This is calculated by taking the density of the mixture into account, unlike C_{H_2O} which is directly determined from the absorbance. Indeed, the mole fraction is the ratio between the mole quantity of water and the mole quantity of mixture. The mole quantity of mixture has been determined from the volume of the cell (fixed during all the experiment) and the density of the mixture from the GERG-2008 equation (Kunz and Wagner, 2012).

Compared with the C_{H_2O} −P plot shown in Fig. 5, the y_{H_2O} −P plot exhibits more complex features which are characterised by the existence of a minimum in y_{H_2O}. For all of the three solubility curves, we can see that y_{H_2O} initially falls with increasing the pressure up to a certain pressure and then rises at high pressures.

When the temperature is above 31.48 °C (upper critical end point of the binary mixture of CO_2 + H_2O; see Wendland et al., 1999) the y_{H_2O} −P curve is a continuous line over a wide pressure range (e.g. from 0.1 to 20 MPa). The observed minimum in y_{H_2O} is

primarily caused by the rapid change of molar density as a function of pressure in the supercritical region. For the pure CO_2 system, the minimum is approximately at 9 MPa, estimated from the solubility data at 40 °C. A similar minimum in y_{H_2O} has been reported previously by Wiebe and Gaddy (1941). Their measurements show that the minimum is located at approximately 8 MPa at 50 °C, which is consistent with the fact of the existence of a minimum in y_{H_2O} at 40 °C, reported in this work. Our new solubility data further confirm that the similar minimum in y_{H_2O} can be observed from the impure CO_2 systems, e.g. addition of 5% or 10% of N_2 in CO_2. Moreover, it can be seen from Table 1 and Fig. 7 that the pressure at the minimum shifts to high pressures as the concentration of N_2 increases: with 5% of N_2 this minimum is found at ca. 10 MPa and at ca. 11 MPa with 10% of N_2.

To obtain smoothed curves of y_{H_2O} versus the system pressure (P), we first fitted the C_{H_2O} –ρ curve for each fluid separately with a polynomial curve, shown in Figs. S1–S3 in the Electronic Supplementary Material. Then the ρ–P relationship calculated from either the Span–Wagner or the GERG-2008 equations was used for converting the C_{H_2O} –ρ plot to the y_{H_2O} –P plot, shown in Fig. 7. Although each C_{H_2O}–ρ plot (Figs. S1–S3) exhibits monotonically increasing values with ρ in the studied density region, the smoothed y_{H_2O}–P curves correctly reproduce the minimum in y_{H_2O} for all of the three systems after applying the ρ–P relationship obtained from the equations of state. Table 1 summarises all the data obtained at 40 °C and presented in Figs. 5–7.

4. Conclusions

In this paper, we have shown that the presence of small percentages of N_2 (5 or 10%) at 40 °C significantly lowers the solubility of water at a given pressure in the range 8–18 MPa. Under these conditions, there are no major changes in phase that might affect the solubility. Furthermore, we have illustrated that the solubility of water follows the same density trend irrespective of the mixture composition. Therefore, the lower solubility of water with higher percentages of N_2 is merely attributed to the reduction in density caused by the presence of N_2.

Preliminary data for CO_2/N_2 medium (with similar mixtures of 5 and 10% of N_2) at 25 °C indicate that same effect is also observed at lower temperature for these dilute CO_2 solutions. Thus, our results suggest that, over the pressure range studied, the solubility of H_2O in dilute solutions of $N_2 + CO_2$ (e.g. $x_{N2} < 10\%$) at a given temperature appears to only depend on the overall density of the fluid. Further studies are required to fully substantiate these initial findings and further work is in progress investigating the effect of other impurities on water solubility in mixtures relevant to CCS.

Acknowledgements

We wish to thank the EPSRC and E.ON for financial support for MATTRAN (Materials for Next Generation CO_2 Transport Systems, E.ON-EPSRC Grant Reference EP/G061955/1) and the UKCCSRC for supporting this work. We thank Julian Barnett from National Grid. We thank Messrs. M. Dellar, M. Guyler, R. Wilson, P. Fields, D. Litchfield, and J. Warren for their technical support. MWG gratefully acknowledges receipt of a Royal Society Wolfson Merit Award.

Appendix A. Supplementary data

Supplementary data associated with this article can be found, in the online version, at doi:10.1016/j.ijggc.2015.02.002.

References

Abbas, Z., Mezher, T., Abu-Zahra, M.R.M., 2013. CO_2 purification. Part I: purification requirement review and the selection of impurities deep removal technologies. Int. J. Greenh. Gas Control 16, 324–334.
Adisasmito, S., Frank, R.J., Sloan, E.D., 1991. Hydrates of carbon dioxide and methane mixtures. J. Chem. Eng. Data 36, 68–71.
Austegard, A., Solbraa, E., de Koeijer, G., Malnvik, M.J., 2006. Thermodynamic models for calculating mutual solubilities in H_2O-CO_2-CH_4 mixtures. Chem. Eng. Res. Des. 84, 781–794.
Bamberger, A., Sieder, G., Maurer, G., 2000. High-pressure (vapor + liquid) equilibrium in binary mixtures of (carbon dioxide + water or acetic acid) at temperatures from 313 to 353 K. J. Supercrit. Fluids 17, 97–110.
Briones, J.A., Mullins, J.C., Thies, M.C., Kim, B.U., 1987. Ternary phase equilibria for acetic acid-water mixtures with supercritical carbon dioxide. Fluid Phase Equilib. 36, 235–246.
Buback, M., 1995. Near infrared spectroscopy of fluid phases. J. Mol. Struct. 347, 113–129.
Buit, L., Ahmad, M., Mallon, W., Hage, F., 2011. CO_2 EuroPipe Study of the Occurrence of Free Water in Dense Phase CO_2 Transport. Energy Procedia, Amsterdam, pp. 3056–3062.
Choi, Y.S., Nesic, S., 2011. Determining the corrosive potential of CO_2 transport pipeline in high pCO2-water environments. Int. J. Greenh. Gas Control 5, 788–797.
Choi, Y.S., Nesic, S., Young, D., 2010. Effect of impurities on the corrosion behavior of CO_2 transmission pipeline steel in supercritical CO_2-water environments. Environ. Sci. Technol. 44, 9233–9238.
Coan, C.R., King Jr., A.D., 1971. Solubility of water in compressed carbon dioxide, nitrous oxide, and ethane. Evidence for hydration of carbon dioxide and nitrous oxide in the gas phase. J. Am. Chem. Soc. 93, 1857–1862.
Cui, Z.D., Wu, S.L., Zhu, S.L., Yang, X.J., 2006. Study on corrosion properties of pipelines in simulated produced water saturated with supercritical CO_2. Appl. Surf. Sci. 252, 2368–2374.
D'Souza, R., Patrick, J.R., Teja, A.S., 1988. High pressure phase equilibria in the carbon dioxide-n-hexadecane and carbon dioxide-water systems. Can. J. Chem. Eng. 66, 319–323.
Davison, J., Thambimuthu, K., 2009. An overview of technologies and costs of carbon dioxide capture in power generation. Proc. Inst. Mech. Eng. A: J. Power Energy 223, 201–212.
de Visser, E., Hendriks, C., Barrio, M., Molnvik, M.J., de Koeijer, G., Liljemark, S., Le Gallo, Y., 2008. Dynamis CO_2 quality recommendations. Int. J. Greenh. Gas Control 2, 478–484.
EASAC, 2013. Carbon capture and storage in Europe. EASAC Policy Report.
Gillespie, P.C., Wilson, G.M., 1982. Vapor–Liquid and Liquid–Liquid Equilibria: Water–Methane, Water–Carbon Dioxide, Water–Hydrogen Sulfide, Water–n-Pentane, Water–Methane–n-pentane, GPA Research Report RR-48.
Goeppert, A., Czaun, M., Surya Prakash, G.K., Olah, G.A., 2012. Air as the renewable carbon source of the future: an overview of CO_2 capture from the atmosphere. Energy Environ. Sci. 5, 7833–7853.
Haszeldine, S.R., 2009. Carbon capture and storage: how green can black be? Science 325, 1647–1652.
Herzog, H.J., 2011. Scaling up carbon dioxide capture and storage: From megatons to gigatons. Energy Econ. 33, 597–604.
Hou, S.X., Maitland, G.C., Trusler, J.P.M., 2013. Measurement and modeling of the phase behavior of the (carbon dioxide + water) mixture at temperatures from 298.15 K to 448.15 K. J. Supercrit. Fluids 73, 87–96.
IEA, 2012. CO_2 Emissions from Fuel Combustion. International Energy Agency.
IEAGHG, 2011. Effects of Impurities on Geological Storage of CO_2. International Energy Agency Greenhouse Gas Programme.
Jackson, K., Bowman, L.E., Fulton, J.L., 1995. Water solubility measurements in supercritical fluids and high-pressure liquids using near-infrared spectroscopy. Anal. Chem. 67, 2368–2372.
Kazarian, S.G., Lawrence, C.J., Briscoe, B.J., 2000. In situ spectroscopy of polymers processed with supercritical carbon dioxide. In: Proceedings of SPIE—The International Society for Optical Engineering. Society of Photo-optical Instrumentation Engineers, pp. 210–216.
Ke, J., Parrot, A.J., Sanchez-Vicente, Y., Fields, P., Wilson, R., Drage, T.C., Poliakoff, M., George, M., 2014. New phase equilibrium analyzer for determination of the vapor-liquid equilibrium of carbon dioxide and permanent gas mixtures for carbon capture and storage. Rev. Sci. Instrum. 85, 085110.
Keeling, C.D., Whorf, T.P., Wahlen, M., Van Der Plicht, J., 1995. Interannual extremes in the rate of rise of atmospheric carbon dioxide since 1980. Nature 375, 666–670.
Keith, D.W., 2009. Why capture CO_2 from the atmosphere? Science 325, 1654–1655.
King, M.B., Mubarak, A., Kim, J.D., Bott, T.R., 1992. The mutual solubilities of water with supercritical and liquid carbon dioxides. J. Supercrit. Fluids 5, 296–302.
Koglbauer, G., Wendland, M., 2008. Water vapor concentration enhancement in compressed humid nitrogen, argon, and carbon dioxide measured by Fourier transform infrared spectroscopy. J. Chem. Eng. Data 53, 77–82.
Kunz, O., Klimeck, R., Wagner, W., Jaeschke, M., 2007. The GERG-2004 wide-range equation of state for natural gases and other mixtures, Düsseldorf.
Kunz, O., Wagner, W., 2012. The GERG-2008 wide-range equation of state for natural gases and other mixtures: an expansion of GERG-2004. J. Chem. Eng. Data 57, 3032–3091.

Lee, Z.H., Lee, K.T., Bhatia, S., Mohamed, A.R., 2012. Post-combustion carbon dioxide capture: evolution towards utilization of nanomaterials. Renew. Sustain. Energy Rev. 16, 2599–2609.

Lemmon, E.W., Huber, M.L., McLinden, M.O., 2007. NIST Standard Reference Data 23 REFPROP Ver. 8.0.

Liu, Y., Hou, M., Ning, H., Yang, D., Yang, G., Han, B., 2012. Phase equilibria of $CO_2 + N_2 + H_2O$ and $N_2 + CO_2 + H_2O + NaCl + KCl + CaCl_2$ systems at different temperatures and pressures. J. Chem. Eng. Data 57, 1928–1932.

Markewitz, P., Kuckshinrichs, W., Leitner, W., Linssen, J., Zapp, P., Bongartz, R., Schreiber, A., Muller, T.E., 2012. Worldwide innovations in the development of carbon capture technologies and the utilization of CO_2. Energy Environ. Sci. 5, 7281–7305.

Nielsen, C.J., Herrmann, H., Weller, C., 2012. Atmospheric chemistry and environmental impact of the use of amines in carbon capture and storage (CCS). Chem. Soc. Rev. 41, 6684–6704.

NIST, 2014. NIST Chemistry WebBook, NIST Standard Reference Database Number 69. National Institute of Standards and Technology, Gaithersburg, MD http://webbook.nist.gov/chemistry/

Pipitone, G., Bolland, O., 2009. Power generation with CO_2 capture: technology for CO_2 purification. Int. J. Greenh. Gas Control 3, 528–534.

Poliakoff, M., Howdle, S.M., Kazarian, S.G., 1995. Vibrational spectroscopy in supercritical fluids: from analysis and hydrogen bonding to polymers and synthesis. Angew. Chem. 34, 1275–1295.

Rubin, E.S., Mantripragada, H., Marks, A., Versteeg, P., Kitchin, J., 2012. The outlook for improved carbon capture technology. Prog. Energy Combust. Sci. 38, 630–671.

Sako, T., Sugeta, T., Nakazawa, N., Okubo, T., Sato, M., Taguchi, T., Hiaki, T., 1991. Phase equilibrium study of extraction and concentration of furfural produced in reactor using supercritical carbon dioxide. J. Chem. Eng. Jpn. 24, 449–455.

Sanchez-Vicente, Y., Drage, T.C., Poliakoff, M., Ke, J., George, M.W., 2013. Densities of the carbon dioxide + hydrogen, a system of relevance to carbon capture and storage. Int. J. Greenh. Gas Control 13, 78–86.

Song, K.Y., Kobayashi, R., 1986. Water Content of CO_2-Rich Fluids in Equilibrium with Liquid Water or Hydrate. Research Report RR-99. Gas Processors Association.

Song, K.Y., Kobayashi, R., 1990. The water content of a CO_2-rich gas mixture containing 5.31 mol% methane along the three-phase and supercritical conditions. J. Chem. Eng. Data 35, 320–322.

Span, R., Wagner, W., 1996. A new equation of state for carbon dioxide covering the fluid region from the triple-point temperature to 1100 K at pressures up to 800 MPa. J. Phys. Chem. Ref. Data 25, 1509–1596.

Spycher, N., Pruess, K., Ennis-King, J., 2003. CO_2-H_2O mixtures in the geological sequestration of CO_2. I. Assessment and calculation of mutual solubilities from 12 to 100 °C and up to 600 bar. Geochim. Cosmochim. Acta 67, 3015–3031.

Stevens, J.G., Gomez, P., Bourne, R.A., Drage, T.C., George, M.W., Poliakoff, M., 2011. Could the energy cost of using supercritical fluids be mitigated by using CO_2 from carbon capture and storage (CCS)? Green Chem. 13, 2727–2733.

Valtz, A., Chapoy, A., Coquelet, C., Paricaud, P., Richon, D., 2004. Vapour-liquid equilibria in the carbon dioxide-water system, measurement and modelling from 278.2 to 318.2 K. Fluid Phase Equilib. 226, 333–344.

Wang, Z., Felmy, A.R., Thompson, C.J., Loring, J.S., Joly, A.G., Rosso, K.M., Schaef, H.T., Dixon, D.A., 2012. Near-infrared spectroscopic investigation of water in supercritical CO_2 and the effect of $CaCl_2$. Fluid Phase Equilib. 338, 155–163.

Wendland, M., Hasse, H., Maurer, G., 1999. Experimental pressure-temperature data on three- and four-phase equilibria of fluid, hydrate, and ice phases in the system carbon dioxide-water. J. Chem. Eng. Data 44, 901–906.

Wiebe, R., 1941. The binary system carbon dioxide-water under pressure. Chem. Rev. 29, 475–481.

Wiebe, R., Gaddy, V.L., 1941. Vapor phase composition of carbon dioxide-water mixtures at various temperatures and at pressures to 700 atmospheres. J. Am. Chem. Soc. 63, 475–477.

Xiang, Y., Wang, Z., Yang, X., Li, Z., Ni, W., 2006. The upper limit of moisture content for supercritical CO_2 pipeline transport. J. Supercrit. Fluids 67, 14–21.